C. R. Mecanique 342 (2014) 96–105

Contents lists available at ScienceDirect

Comptes Rendus Mecanique

www.sciencedirect.com

Limit analysis and lower/upper bounds to the macroscopic criterion of Drucker–Prager materials with spheroidal voids

Franck Pastor [a], Djimedo Kondo [b,*]

[a] Athénée royal Victor-Horta, rue de la Rhétorique, 16, Bruxelles, Belgium
[b] Institut Jean-Le-Rond-d'Alembert, UMR 7190 CNRS, UPMC, 75252 Paris cedex 05, France

ARTICLE INFO

Article history:
Received 7 October 2013
Accepted 11 December 2013
Available online 16 February 2014

Keywords:
Gurson-type models
Spheroidal voids
Micromechanics
Limit analysis
Upper and lower bounds
Conic programming

ABSTRACT

The paper is devoted to a numerical Limit Analysis of a hollow spheroidal model with a Drucker–Prager solid matrix, for several values of the corresponding friction angle ϕ. In the first part of this study, the static and the mixed kinematic 3D-codes recently evaluated in [1] are modified to use the geometry defined in [2] for spheroidal cavities in the context of a von Mises matrix. The results in terms of macroscopic criteria are satisfactory for low and medium values of ϕ, but not enough for $\phi = 30°$ in the highly compressive part of the criterion. To improve these results, an original mixed approach, dedicated to the axisymmetric case, was elaborated with a specific discontinuous quadratic velocity field associated with the triangular finite element. Despite the less good conditioning inherent to the axisymmetric modelization, the resulting conic programming problem appears quite efficient, allowing one take into account numerical discretization refinements unreachable with the corresponding 3D mixed code. After a first validation in the case of spherical cavities whose exact solution is known, the final results for spheroidal voids are given for three usual values of the friction angle *and two values of the cavity aspect factor*.

1. Introduction

The famous Gurson plasticity criterion [3] is based on the consideration of a hollow von Mises sphere or cylinder in the framework of the Limit Analysis (LA) kinematic approach. Recent studies were devoted to porous materials with a matrix exhibiting a pressure-sensitive behavior ([4–6], etc.). Several extensions of the Gurson model taking into account void-shape effects have been also proposed in order to solve various practical cases such as penny-shaped crack-like voids (see, among others, [7–12]). Up to our knowledge, similar theoretical studies with pressure-sensitive matrices and non-spherical voids do not exist in the literature. There is still need for an appropriate research effort in order to extend available efficient models (for instance the one proposed by [5]) to the case of spheroidal voids.

On the other hand, using finite-element discretizations, both static and kinematic methods of LA have been elaborated for Gurson problems with cylindrical cavities [13–15]. In the subsequent work [16], the Gurson criterion (then with a von Mises matrix) is shown to be relevant for materials with spherical voids by using the same tools and an original three-dimensional numerical model. Using also the hollow sphere model, a recent paper [1] was devoted to porous materials with pressure-sensitive matrices obeying the Drucker–Prager, Mises–Schleicher and Green criteria. Also, in the case of a von Mises matrix, these numerical studies have been extended to take into account void shape effects by considering central spheroid voids in matrices with a confocal boundary [2]. They concluded on the relevance of the criteria proposed by the above-mentioned studies of Gologanu and Leblond, at least for the investigated porosity cases.

* Corresponding author.
E-mail addresses: franck.pastor@skynet.be (F. Pastor), djimedo.kondo@upmc.fr (D. Kondo).

1631-0721/$ – see front matter
http://dx.doi.org/10.1016/j.crme.2013.12.002

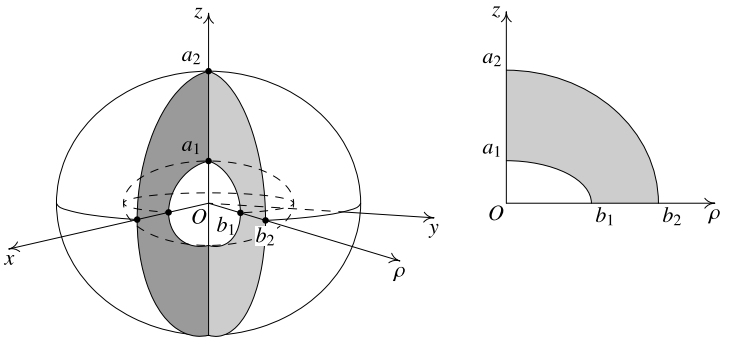

Fig. 1. The hollow spheroid model ($a_1/b_1 = 0.5,\ f = 0.1$).

The main advantage of these LA numerical approaches is that they provide rigorous, *a posteriori* controllable bounds to the macroscopic criterion. Therefore, the purpose of the present paper is to provide lower and upper bound results to be used as reference values for forthcoming attempts to determine approximate criteria for porous Drucker–Prager materials with oblate cavities in the framework of LA applied to the hollow spheroid model.

The paper is organized as follows. First, we briefly present the considered hollow spheroid problem and its formulation in terms of LA. Then, we recall the basis of the static and mixed methods of LA, and we recall the corresponding expressions for the Drucker–Prager material needed to obtain the bounds and to assess them by post-analysis of the optimal fields. The next step is devoted to detail the proposed original formulation of the mixed (but rigorously kinematic) method focused on the axisymmetric case. Let us note also that it is the first time that the LA mixed approach is applied to an axisymmetric finite element problem, even in its usual form where the lower/upper bound status of the solution is generally not guaranteed. Finally, we give the results of the 3D and axisymmetric tests for three usual values of the friction angle defined by identifying Drucker–Prager and Coulomb criteria in plane strain as detailed in [17]. The resulting graphs also allow us point out the evolution of the macroscopic criterion with the friction angle, for two usual values of the aspect factor of the cavity.

2. The hollow spheroid model

The hollow spheroid model is made up of a single spheroidal cavity embedded in a confocal spheroidal cell. The solid matrix is an isotropic, homogeneous, and rigid-plastic Drucker–Prager material. Fig. 1 presents the geometric model, where the given aspect ratio a_1/b_1 and porosity f allow us determine the parameters a_2 and b_2 of the confocal spheroidal boundary. Let us consider first the three-dimensional point of view, and note Σ and D the macroscopic stress and strain rate tensors. These quantities are related to the microscopic fields by the averages over the model of volume V:

$$\Sigma_{ij} = \frac{1}{V}\int_V \sigma_{ij}\,\mathrm{d}V, \qquad D_{ij} = \frac{1}{2V}\int_{\partial V}(u_i n_j + u_j n_i)\,\mathrm{d}S \tag{1}$$

where u denotes the velocity vector and n the normal vector to the boundary ∂V of the model.

Under the uniform strain boundary conditions, i.e. $u_i = D_{ij}x_j$ (in which x represents the position vector), on the external boundary, the overall virtual dissipated power $P_{\text{tot}} = \Sigma_{ij}D_{ij}$ can be written as follows:

$$P_{\text{tot}} = V\,Q\cdot q \tag{2}$$

where the loading vector Q and the generalized velocity q here are defined as:

$$Q_1 = \Sigma_m = \frac{1}{3}(\Sigma_x + \Sigma_y + \Sigma_z), \qquad Q_2 = \frac{\Sigma_x + \Sigma_y}{2} - \Sigma_z, \qquad Q_3 = \frac{\sqrt{3}}{2}(\Sigma_x - \Sigma_y)$$
$$Q_4 = \Sigma_{yz}, \qquad Q_5 = \Sigma_{zx}, \qquad Q_6 = \Sigma_{xy}$$
$$q_1 = (D_x + D_y + D_z), \qquad q_2 = \frac{2}{3}\left(\frac{D_x + D_y}{2} - D_z\right), \qquad q_3 = \frac{1}{\sqrt{3}}(D_x - D_y)$$
$$q_4 = 2D_{yz}, \qquad q_5 = 2D_{zx}, \qquad q_6 = 2D_{xy}$$

From the matrix isotropy and the spheroidal geometry of the model, the resulting material is transversally isotropic around the axis z. Here is investigated the macroscopic criterion $g(\Sigma)$ in the $(Oxyz)$ anisotropy frame. As in [2], we search for the projection of $g(\Sigma)$ in the (Q_1, Q_2) plane by optimizing Q_2 for fixed $Q_1 = \Sigma_m$, other stress components defined in (2) being free. Then, $\frac{\partial g}{\partial \Sigma_{ij}} = 0 = 2D_{ij}$ for $i \neq j$, and $\frac{\partial g}{\partial Q_3} = 0 = q_3$, since the macroscopic material complies to the normality rule. Finally, loadings can be restricted to the principal macroscopic strain rates D, as well as Σ since $(Oxyz)$ is a transverse isotropy frame, with $D_x = D_y$.

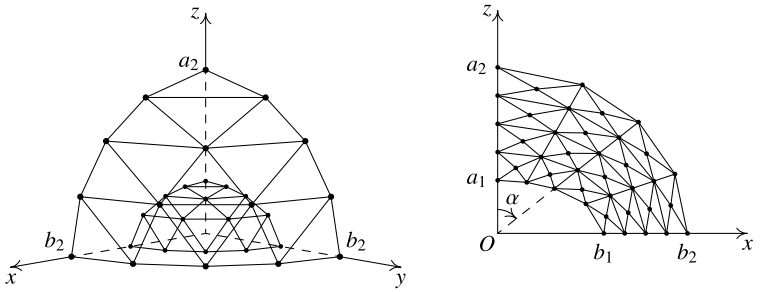

Fig. 2. General view of an 896-tetrahedron mesh ($a_1/b_1 = 0.5$, $f = 0.1$) (left), and the corresponding axisymmetric mesh by substituting ρ to x (right).

Moreover, all the axes in the horizontal plane of Fig. 1 are equivalent; therefore, in the projection problem, we have also $\Sigma_x = \Sigma_y$. From these results, the problem can be analyzed also as axisymmetric by using the (ρ, z) frame. Finally, the overall external power P_{tot} depends only on the two non-zero loading parameters Q_1 and Q_2. Therefore, adapting the technique defined in [16] for spherical cavities, the eighth of the hollow spheroid is meshed into tetrahedral elements as shown in Fig. 2 left in the 3D case. Note that the macroscopic equivalent stress Σ_{eq} is, in the present case where $\Sigma_x = \Sigma_y = \Sigma_\rho$, linked to Q_2 by:

$$\Sigma_{\text{eq}} = \sqrt{\frac{3}{2}\Sigma' : \Sigma'} = |Q_2| = |\Sigma_x - \Sigma_z| \tag{3}$$

where Σ' is the deviatoric part of Σ. From this analysis, the mechanical problem can be considered as axisymmetric in the cylindrical (ρ, θ, z) frame of Fig. 2 right by substituting ρ to x in the horizontal axis. In this case, we can substitute in the above relations Σ_ρ to Σ_x and to Σ_y (Σ_z unchanged), and D_ρ to D_x and D_y. The loading conditions $u_i = D_{ij}x_j$ here become $u_\rho = D_\rho \rho$, $u_z = D_z z$.

From the results of the comparative study of [1] for spherical cavities, we have first extended the 3D static and mixed finite element codes by implementing the geometric meshing of [2]; such procedure is not detailed here. To overcome the drawback of the excessive amount of CPU times required to sufficiently improve these 3D results, we have elaborated an original axisymmetric version of the mixed kinematic approach based on specific quadratic velocities in the triangular elements. This mixed formulation avoids the possible singularities of the axisymmetric formulation together with using convexity properties in order to preserve the character of rigorous upper bound of the final results. Hereafter, we fully detail the axisymmetric mixed method and its application to the present problem. The final – 3D and axisymmetric – resulting graphs are presented for three usual values of the friction angle.

3. LA methods and Drucker–Prager criterion

The main goal of limit analysis is the determination of the limit load locus that corresponds to the macroscopic plasticity criterion in the present micro–macro problem. Classically, the limit loads can be determined by using a static (or lower bound) and a kinematic (or upper bound) methods.

3.1. The static method

The first one is the static method which is in terms of stresses and leads to a lower bound of the limit loads. A stress field is said admissible if it is statically admissible (SA), and plastically admissible (PA), i.e. verifying the (convex) plasticity criterion $f(\sigma)$; a loading vector $Q(\sigma)$ is admissible if the corresponding σ is admissible. Let us denote by K the set of the admissible loading vectors. The final problem reads:

$$Q_{\text{lim}} = \left(Q_1^d, \ldots, \lambda_0 Q_i^d, \ldots, Q_n^d\right) \tag{4i}$$

$$\lambda_0 = \max\left\{\lambda,\, Q(\sigma) = \left(Q_1^d, \ldots, \lambda Q_i^d, \ldots, Q_n^d\right)\right\} \tag{4ii}$$

where the stress tensors σ are admissible, and Q^d is a fixed admissible loading vector. In fact, relation (4) holds when all admissible fields σ can be taken into account, which is not the case in general. Then, by varying the direction of Q_d, a set of admissible Q, located near or on ∂K, is obtained: the smallest convex envelope of the corresponding points in K is an inner approach of the boundary ∂K, i.e. a lower bound to the exact macroscopic criterion investigated here.

3.2. The mixed kinematic method

On the other hand, a so-called mixed kinematic formulation was pioneered by Anderheggen and Knopfel [18] for finite-element continuous velocity and a linearized von Mises criterion. An extension to the discontinuous velocity case, based on

the assumption that linear programming duality properties remain valid in non-linear programming, was proposed in [19]. A general extension to discontinuous velocities and convex optimization was successfully experienced in [20] and [21] for homogeneous von Mises and Gurson materials in plane strain. This mixed formulation is here modified as:

$$\max_{Q,\sigma,T'} F = V q_d \cdot Q \tag{5i}$$

$$\text{s.t.} \int_V d:\sigma \,\mathrm{d}V + \int_{S_d} [u]\cdot T' \,\mathrm{d}S = V q(u)\cdot Q \quad \forall \mathrm{KA}\, u, \tag{5ii}$$

$$f(\sigma) \leqslant 0, \quad f_{nt}(T') \leqslant 0 \tag{5iii}$$

where d is the strain rate tensor, σ the stress tensor, S_d the union of the velocity discontinuity surfaces, T' the stress vector on these surfaces and $f_{nt}(T')$ the projection of $f(\sigma')$ on the Mohr plane associated with the discontinuity surface of normal n. In (5), the velocity field u must be kinematically admissible (KA), i.e. locally continuous with bounded discontinuities $[u]$, and verifying the boundary conditions together with the loading condition $q(u) = q^d$. It can be seen in the above-mentioned papers that the optimal velocity field will also be PA (plastically admissible), i.e. there exists everywhere a tensor σ or a vector T' associated with the strain rate tensor or to the velocity jump by the normality law corresponding to $f(\sigma) = 0$ and $f_{nt}(T') = 0$ respectively.

The previous formulation gives the exact solution if all velocity and stress fields could be taken into account. In general, this is not the case when we consider a discretization of the mechanical system in finite elements. However, the following axisymmetric formulation is formulated for preserving the rigorous kinematic (or upper bound) character of the final result by using convexity properties concerning the set of PA strain rate (and velocity jump) fields and the unit dissipated powers.

3.3. The Drucker–Prager material

The Drucker–Prager criterion reads (with $\mu \geqslant 0$):

$$f(\sigma) = \sigma_{\mathrm{eq}} + \mu\sigma_m - \sigma_0 \leqslant 0; \quad \sigma_{\mathrm{eq}} = \sqrt{\frac{3}{2}\sigma' : \sigma'} \tag{6}$$

where σ' is the deviatoric stress tensor, σ_{eq} the von Mises equivalent stress, σ_m the mean stress $\mathrm{tr}(\sigma)/3$, σ_0 the flow stress under pure shear ($\sigma_m = 0$) and μ the pressure sensitivity factor.[1]

From the projection of the criterion (6) on the Mohr plane, we obtain the corresponding criterion:

$$f_{nt}(T) = \sqrt{3a}\,|\sigma_{nt}| + \mu\sigma_n - \sigma_0 \leqslant 0; \quad a = 1 - 4\mu^2/9 \tag{8}$$

which gives the usual Coulomb criterion in the Mohr plane by using the formulas (7). The kinematic PA condition and the unit dissipated power $\pi(d)$ for the strain rate field read:

$$\mathrm{tr}(d) \geqslant \mu\, d_{\mathrm{eq}}, \quad d_{\mathrm{eq}} = \sqrt{\frac{2}{3} d' : d'}; \qquad \pi_{\mathrm{vol}}(d) = \frac{\sigma_0}{\mu}\mathrm{tr}(d) \tag{9}$$

where d' is the deviatoric part of the strain rate tensor d. From (9), the domain of the PA strain rates is a convex cone whose apex corresponds to the null tensor.

The corresponding PA conditions on the discontinuities read:

$$[u_n] \geqslant \frac{\mu}{\sqrt{3a}}\big|[u_t]\big|; \qquad \pi_{\mathrm{disc}}\big([u]\big) = \frac{\sigma_0}{\mu}[u_n] \tag{10}$$

which gives the usual formulas in terms of c, ϕ constants with $\tan\phi = \mu/\sqrt{3a}$ and $c = \sigma_0/\sqrt{3a}$. The expressions (9) and (10) here are only used in the post-analysis of the optimal solution of the mixed method.

4. Numerical implementation of the axisymmetric mixed method

Fig. 2 left illustrates the case of the 3D-mesh with four layers of triangle-based prisms, each layer constituted by 4×4 prisms of 3×4 tetrahedrons and two extremal tetrahedrons each, i.e., 896 tetrahedrons for the whole mesh. The corresponding axisymmetric mesh in the frame (ρ, z) is given on the right with four sectors ($n_s = 4$) and four layers ($n_\rho = 4$). For each aspect ratio a_1/b_1 of the cavity and for a given porosity, the matrix boundaries of the spheroid mesh are adapted to obtain their confocal forms. Since these boundaries are not homothetic, the porosity of the resulting mesh is not exactly the input one. Therefore, in a first step for each case of porosity and aspect ratio, the distribution of the angle α is optimized to retrieve the desired porosity by progressively concentrating this distribution towards the more curved zone.

[1] The usual geotechnical constants (cohesion c, and friction angle ϕ), as defined in [17], can be obtained by the following relationships:

$$\beta = \mu/\sqrt{27}; \qquad \sin\phi = 3\beta/\sqrt{(1-3\beta^2)}; \qquad c = \sigma_0\sqrt{3\big(3+\sin^2\phi\big)}/(\sqrt{27}\cos\phi) \tag{7}$$

4.1. The virtual velocity field

In each triangle, the FEM discontinuous displacement velocity field is expressed as follows:

$$\begin{cases} u_\rho = \rho(A + B\rho + Cz) \\ u_\theta = 0 \\ u_Z = D + E\rho + Fz + H\rho z + I\rho^2 + Jz^2 \end{cases} \tag{11}$$

$$d_\rho = \frac{\partial u_\rho}{\partial \rho}; \qquad d_\theta = \frac{u_\rho}{\rho}; \qquad d_z = \frac{\partial u_z}{\partial z}; \qquad d_{\rho z} = \frac{1}{2}\left(\frac{\partial u_\rho}{\partial z} + \frac{\partial u_z}{\partial \rho}\right) \quad \Rightarrow \quad \{d\} = [B]\{X\} \tag{12}$$

Thus, each triangle generates nine constants ($X_i = A, B, \ldots, J$), which are the final virtual variables of the discretized model. The resulting strain rate field inside the triangle can be easily cast into the form $\{d(\rho, z)\} = [B(\rho, z)]\{X\}$ where the components of X are the (virtual) variables of the triangle. From this choice, the resulting strain rate tensor d cannot become singular and it is linearly varying in the element: this feature will be used later to (strictly) upper bound the (convex) unit dissipated power on the triangle.

Along an inter-element side, the velocity jump $[u]$ is quadratic. To upper bound as above the corresponding dissipated power, the jump is linearized by enforcing the jump at the side middle to be equal to half the sum of its values at the ends of the discontinuity. Note that an interesting methodology for maintaining the PA character of a quadratic $[u]$ along the discontinuity is given in [22], but it is not easily applicable when using the present mixed method. *It is worth also noting that, in the LA numerical literature for axisymmetric problems, the drawback of the singularity at the origin is avoided by enforcing the PA conditions only at the centroid of the element, giving by the way only an estimate of the real solution.*

4.2. Formulation of the virtual power principle (5ii)

4.2.1. Contribution of the element velocity fields

The first part of the integral in (5ii) here becomes, for a triangle of volume V:

$$P_V = \int_V d : \sigma \, \mathrm{d}V = 2\pi \int_V \{d\}^t \{\sigma\} \rho \, \mathrm{d}\rho \, \mathrm{d}z \tag{13}$$

As detailed in [1,20], from the Karush–Kuhn–Tucker optimality conditions, the product $\{d\}^t\{\sigma\}$ becomes the convex unit dissipated power $\pi_V(d)$ in the optimal solution. Then, to this product we substitute its linear interpolation $\mathcal{L}(\{d\}^t\{\sigma\})$ between its values at each vertex of the triangular element. Since the product $\rho\mathcal{L}$ is quadratic, the integral $\int \rho\mathcal{L}\,\mathrm{d}\rho\,\mathrm{d}z$ is classically calculated from its values at the medium of the sides of the triangle. Since each term of the product is linear, the final result depends only on the product values at the element vertices. Hence, a stress tensor $\{\sigma\} = (\sigma_\rho, \sigma_z, \sigma_\theta, \sigma_{\rho z})^{\mathrm{T}}$ is assigned at each vertex of the triangle, *without any variation assumption*.

We finally obtain for the triangle with vertices $i = 1$ to 3 and area A:

$$P_V \leqslant \frac{\pi A}{6} \sum_{i=1,3} C_i \{d\}_i^t \{\sigma\}_i \tag{14}$$

where $C_i = 2\rho_i + \rho_{i+1} + \rho_{i+2}$, with $\rho_4 = \rho_1$ and $\rho_5 = \rho_2$.

It is important to note that the strain rate d of the optimal solution will result in PA at the vertices of the triangle; from the convexity of the set of PA strain rates associated with the present (convex) criterion, and from the linear variation of d in (12), it can be deduced that the strain rate will be PA all over the element, a *sine qua non* condition for preserving the upper bound character of the result.

4.2.2. Contribution of the velocity discontinuities

The second part of the integral in (5ii) is the sum of the power contribution of each discontinuity surface L_{1-2} (of ends noted 1 and 2):

$$P_d = \int_{L_{1-2}} [u] \cdot T' \, \mathrm{d}S = 2\pi \int_{L_{1-2}} \left\{[u]\right\}^t \left\{T'\right\} \rho \, \mathrm{d}\rho \, \mathrm{d}z \tag{15}$$

According to [17], the product $[u] \cdot T'$ becomes the dissipated power $\pi_d([u])$ when the stress vector T' and the velocity jump vector $[u]$ are associated (by the normality law) relatively to the $f_{nt}(T')$ criterion. Here also, we can use the convexity of $\pi_d([u])$ since $[u]$ is constrained to vary linearly along the discontinuity side: to the product $\{[u]\}^t\{T'\}$ we substitute its linear interpolation $\mathcal{L}(\{[u]\}^t\{T'\})$ between its values at each end of the discontinuity side of normal n. Then we can upper bound P_d by calculating the quadratic expression with Simpson formula and using the linearity of each term of the

product $\rho\mathcal{L}$. By allocating an auxiliary stress vector $T' = (\sigma_{nn}, \sigma_{nt})$ (expressed in the orthonormal (n, t) frame of the side) at each of the two apices of the discontinuity side L_{1-2}, we finally obtain:

$$P_d \leqslant \frac{2\pi l}{6} \sum_{i=1,2} C_i \left(\{[u]_i\}^t \{T'_i\} \right) \tag{16}$$

where l is the length of L_{1-2}, $C_i = 2\rho_i + \rho_{i+1}$ with $\rho_3 = \rho_1$. It can be noted that the optimal jump $[u]$ will be PA all along L_{1-2} from the convexity of the PA jump set associated with the criterion f_{nt}.

4.2.3. Expression of the external power

To the global vector of the virtual u-velocities are added the generalized velocities q_1, q_2, q_3 in order to form the final virtual vector $\{u\}$. Thus, from (2), the external power can be written as:

$$P_{\text{ext}} = V(q \cdot Q) = V\{q\}^{\mathrm{T}}\{Q\} = \{u\}^{\mathrm{T}} V[\beta]\{Q\} \tag{17}$$

where $\{q\} = [\beta]^{\mathrm{T}}\{u\}$.

4.2.4. The PA stress conditions

In the global (x, y, z) reference frame, the Drucker–Prager yield condition (6) is now written as:

$$\sqrt{\left(\frac{\sigma_{\rho\rho} + \sigma_{zz}}{2} - \sigma_{\theta\theta} \right)^2 + \frac{3}{4}(\sigma_{\rho\rho} - \sigma_{zz})^2 + 3\sigma_{\rho z}^2} \leqslant \sigma_0 - \mu\sigma_m \tag{18}$$

Criterion (18) can be easily written in the Lorentz form required by the conic optimizer MOSEK [23]:

$$\sqrt{x_1^2 + x_2^2 + x_3^2} \leqslant x_4, \quad x_4 = \sigma_0 - \mu\sigma_m \tag{19}$$

for each vertex of the triangle elements.

The criterion (8) for the stress vector T' gives rise to the following inequalities, using (7):

$$\sigma'_{nt} + \sigma'_{nn} \tan\phi \leqslant c, \qquad -\sigma'_{nt} + \sigma'_{nn} \tan\phi \leqslant c \tag{20}$$

which results in two linear constraints in terms of the real variables σ'_{nn} and σ'_{nt} for each end of the discontinuity sides.

4.2.5. The final mixed problem and the KA conditions

Finally, the numerical form of the variational mechanical problem (5) is as following:

$$\begin{aligned} &\text{Max } V\{q_d\}^{\mathrm{T}}\{Q\} \\ &\text{s.t. } -[\alpha]\{\sigma\} - \left[\alpha'\right]\left\{T'\right\} + V[\beta]\{Q\} = 0 \\ &f(\sigma) \leqslant 0 \quad \forall\sigma;\ f_{nt}\left(T'\right) \leqslant 0 \quad \forall T' \\ &+ \text{KA velocity conditions} \end{aligned} \tag{21}$$

Indeed, a systematic change of d and u in terms of the final $\{X\}$ virtual variables is performed through specific subroutines of the axisymmetric Fortran code, which generates the final problem in the MPS format required by MOSEK.

As shown in the detailed analysis of [1] and [20], we can identify the dual variables of the solution of this optimization problem with the $\{X\}$ components. This analysis also details how the resulting velocity field is plastically admissible and how, by adding auxiliary columns, the kinematically admissible character of the optimal velocity field can be ensured, as in the following.

- We previously defined two supplementary rows (constraints) whose associated virtual variables are q_1, q_2 and two new columns for the corresponding macroscopic stresses Q_1, Q_2. At each apex and at the middle of the boundary triangle sides, we impose the loading conditions $u_\rho = D_\rho \rho$, $u_z = D_{zz} z$. This is done by adding one additional column (i.e., an additional variable) for each one of these conditions. Let us note the chosen kinematic parameters as $\{q\} = [A_D]\{D\}$ with $\{D\}^{\mathrm{T}} = (D_\rho, D_z)$; then, for example, the terms of a condition $u_\rho - \rho D_\rho = 0 \Rightarrow u_\rho - \rho[A_D]^{-1}\{q\} = 0$ are dispatched on the (X, q) components (corresponding to u_ρ and q) of the additional column.
- A similar technique is used to impose the null symmetry value to the u_z components on the ρ axis, and to enforce the jump $[u]$ of the middle of the discontinuity side to be equal to half the sum of its end values.

Table 1
Comparison of Σ_m exact values to those obtained by the numerical methods – Drucker–Prager matrix – spherical void – porosity $f = 0.1$ – cohesion $c = 1$.

	Friction angle ϕ	10°	20°	30°
Compression	3D-MEF static	−4.3493	−8.8961	−27.6125
	Exact value	−4.3961	−9.0408	−28.764
	Axi-mixed kinematic	−4.4052	−9.0688	−28.9607
	3D-mixed kinematic	−4.4076	−9.0938	−29.287
Tension	3D-MEF static	1.7944	1.2986	0.9676
	Exact value	1.8045	1.3031	0.9704
	Axi-mixed kinematic	1.8060	1.3039	0.9709
	3D-mixed kinematic	1.8065	1.3045	0.9714

5. Numerical tests and evaluation of existing macroscopic criteria

5.1. Comparison with exact results for spherical voids

Table 1 gives the values obtained with the 3D and axisymmetric codes for isotropic loadings (i.e. $Q_2 = 0$) in tension and compression, together with the exact values given in [24] for spherical cavities. All these runs were performed using two processors. The axisymmetric code was run on an Apple Mac Book Pro with a 2.8 GHz Core 2 Duo and 8 gigabytes of RAM. The final mesh of 10,404 triangles gives a conic problem with a constraint matrix involving 280,503 rows, 374,393 columns, and 93,432 Lorentz cones; the problem is solved in less than one minute by the 32 bits 5th release of MOSEK. The 3D static and kinematic tests were made on a recent Apple Mac Pro with 32 Gbytes of RAM, each run needing about 2000 to 4500 s.

It can be noted first that the 3D bounds are in general close to the exact values, but in a lesser extent for $\phi = 30°$ and compressive loadings. The axisymmetric code appears more efficient than the 3D kinematic one; this performance is mainly due to the quadratic variation of the velocity field and the very smaller size of the final problem for a given polygonal approximation of the matrix boundary. It can be also noted that the linearization of the velocity discontinuities, in order to preserve the kinematic character of the method, has not significatively decreased the performance in terms of upper bound results.

5.2. Application to the Drucker–Prager material with oblate voids

In all the tests, the porosity is taken as 0.1. We consider first the case of the 0.2 aspect factor a_1/b_1 where both 3D and axisymmetric kinematic models are used, together with the 3D static codes for the lower bound approach. From the comments about these results, the case of the aspect factor 0.5 is afterwards investigated by using the axisymmetric and the static code.

5.2.1. Case $a_1/b_1 = 0.2$ and discussion

In Figs. 3–5 are shown the results for a spheroidal cavity having an aspect ratio $a/b = 0.2$. A porosity $f = 0.1$ and friction angles $\phi = 10$, 20 and 30 degrees are considered for the Drucker–Prager matrix. Recalling that this problem has not been studied in the literature up to now, we present the axisymmetric results to be compared to the 3D static and kinematic ones. It should be useful to remember that the present axisymmetric mixed bounds are also strict upper bounds when considering the general 3D problem. First of all, it can be seen that the kinematic and static bounds always remain correctly ordered; note that it was already the case even when the bounds were very close, as in Table 1 corresponding to spherical cavities. For the small values of the friction angle, the macroscopic plasticity criterion appears accurately defined. For friction angle values greater than 20°, the axisymmetric results noticeably reduce the gap between the 3D bounds for high compressive loadings. From the features of the axisymmetric code that allowed also a very refined mesh, it seems that the next step should be devoted to use more refined static meshes, however without changing the linear variation of the element stresses which are necessary to obtain rigorous lower bounds.

Comments. A question arises from the previous kinematic results: is it possible to obtain the mixed axisymmetric results by sufficiently increasing the mesh refinement of the 3D mixed approach?

In Table 2, a comparison between the two kinematic codes has been conducted until the size limit enhanced by MOSEK, on the case $\phi = 30$ and $Q_2 = 0$ where the bounds are less close. It can be seen that increasing – regardless of the computation time – the size of the 3D-mesh does not induce a convergence to the axisymmetric value.

However, the 3D approach does not lose all its interest since it allows non-axisymmetric loading. Indeed, the axisymmetric hypothesis removes a part of the performance added by the 3D transverse discontinuities, but not enough to obtain better results with the 3D model, even by disproportionately refining the FEM mesh.

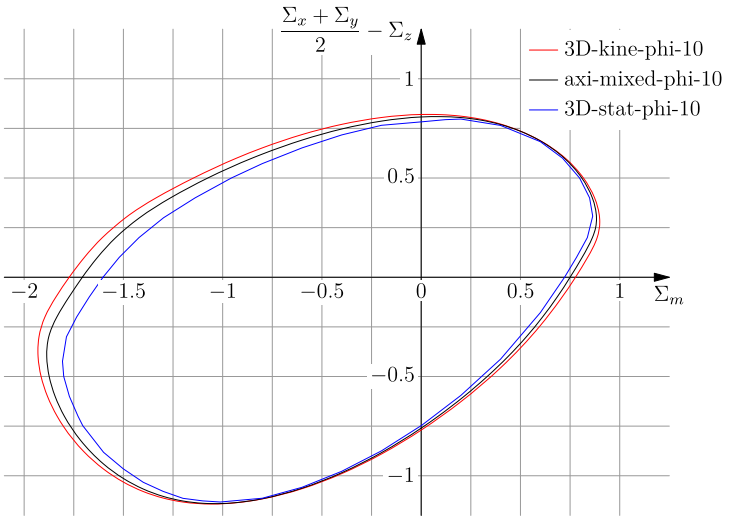

Fig. 3. (Color online.) Present results – Drucker–Prager matrix – $f = 0.1$; $a_1/b_1 = 0.2$ – $\phi = 10°$; $\sigma_0 = 1$.

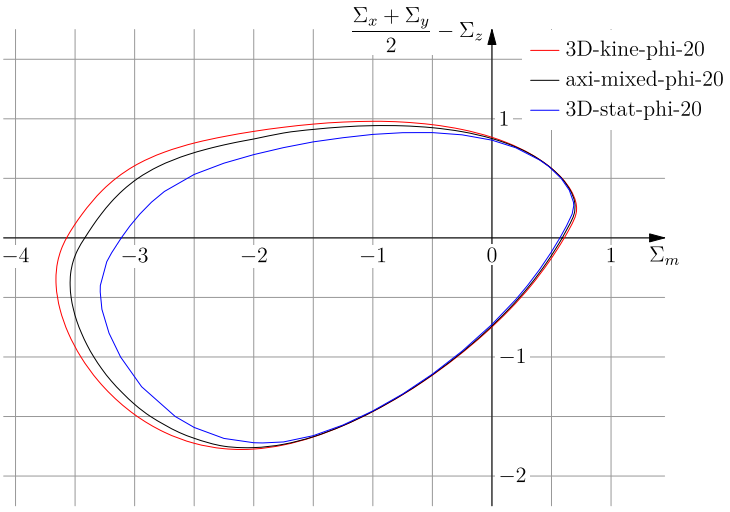

Fig. 4. (Color online.) Present results – Drucker–Prager matrix – $f = 0.1$; $a_1/b_1 = 0.2$ – $\phi = 20°$; $\sigma_0 = 1$.

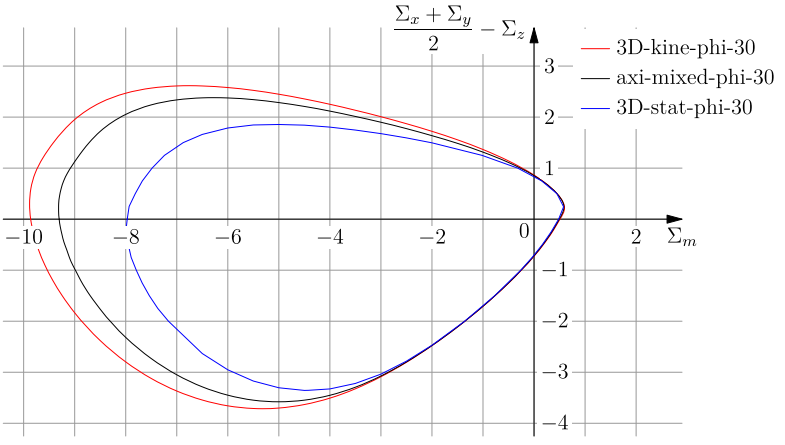

Fig. 5. (Color online.) Present results – Drucker–Prager matrix – $f = 0.1$; $a_1/b_1 = 0.2$ – $\phi = 30°$; $\sigma_0 = 1$.

Table 2
Comparison of axisymmetric and 3D methods – 8 core used – Drucker–Prager matrix – oblate void – $f = 0.1$; $a_1/b_1 = 0.2$; $\phi = 30°$ – $Q_2 = 0$; $\sigma_0 = 1$.

	n_s–n_ρ	17–17	21–21	24–24	26–26	51–51
3D code	tetrahedrons	68,782	129,654	193,536	246,064	1,857,114
	Min Q_1	−9.8626	−9.6971	−9.6153	−9.5645	–
	CPU time	2500 s	9207 s	12,202 s	18,766 s	–
Axi. code	triangles	1156	1764	2304	2704	10,404
	Min Q_1	−9.9995	−9.7584	−9.6426	−9.5870	−9.3022
	CPU time	<2 s	2 s	5 s	6 s	18 s

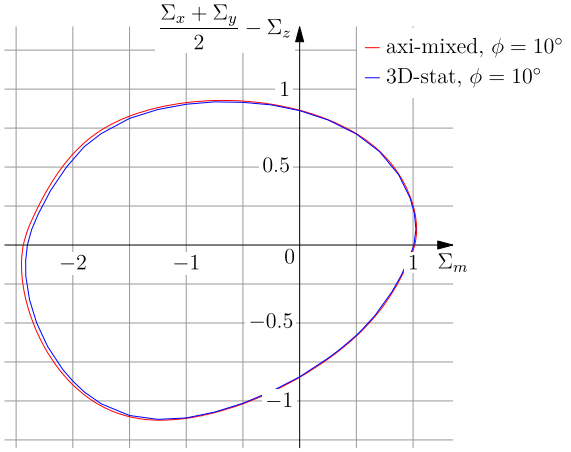

Fig. 6. (Color online.) Present results – Drucker–Prager matrix – $f = 0.1$; $a_1/b_1 = 0.5$ – $\phi = 10°$; $\sigma_0 = 1$.

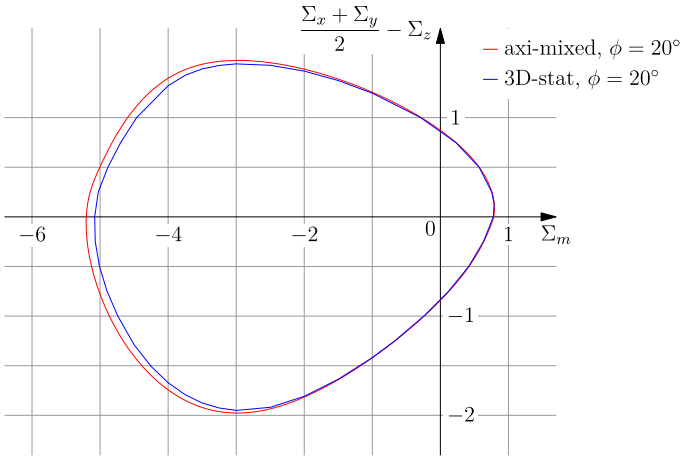

Fig. 7. (Color online.) Present results – Drucker–Prager matrix – $f = 0.1$; $a_1/b_1 = 0.5$ – $\phi = 20°$; $\sigma_0 = 1$.

5.2.2. Case $a_1/b_1 = 0.5$

From the above-mentioned comments, we give here the same tests for the aspect factor 0.5 and the three previous values of the friction angle, using only the axisymmetric and the 3D static codes. (See Figs. 6–8.) In this case, as expected but not in this extent, the bounds appear noticeably closer than in the previous aspect factor study. In all the tests, even when the bounds are almost coincident, they are here also in the good order, all results being controlled by a systematic post-analysis of the optimal solution.

6. Conclusion

The main purpose of the present paper was to provide numerical, but rigorous bounds to the macroscopic criterion of a "porous Drucker–Prager material" with oblate voids, a problem not studied in the literature up to now, at least to our knowledge. These bounds, not only allow us to understand and characterize the macroscopic plastic properties of the above

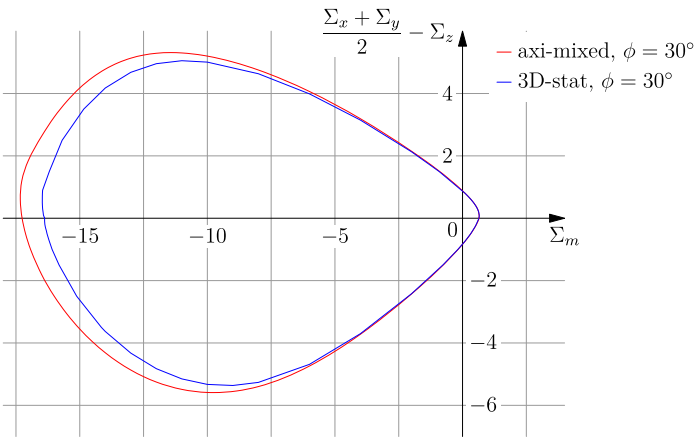

Fig. 8. (Color online.) Present results – Drucker–Prager matrix – $f=0.1$; $a_1/b_1=0.5$ – $\phi=30°$; $\sigma_0=1$.

class of materials, but are also expected to serve as reference results for forthcoming theoretical investigations. To improve the results obtained with a first series of tests with 3D-codes specifically adapted, an original mixed axisymmetric approach has been elaborated. The resulting code has allowed a noticeable improvement of the kinematic bounds by using specific quadratic velocity fields together with FEM refinements of the problem unreachable with the 3D version. After a validation in the spherical case where the exact solution is known, the graphs relative to the macroscopic plasticity criterion are given for three usual values of the friction angle and two values of the cavity aspect factor; they highlight, among others, the evolution of the plasticity criterion depending on the friction angle. Based on the present numerical results, it appears that the next step should be a decomposition of the static approach in order to improve now the lower bound approach.

References

[1] F. Pastor, D. Kondo, J. Pastor, 3D-FEM formulations of limit analysis methods for porous pressure-sensitive materials, Int. J. Numer. Methods Eng. 95 (2013) 847–870.
[2] F. Pastor, D. Kondo, Assessment of hollow spheroid models for ductile failure prediction by limit analysis and conic programming, Eur. J. Mech. A, Solids 38 (2013) 100–114.
[3] A.L. Gurson, Continuum theory of ductile rupture by void nucleation and growth – part I: yield criteria and flow rules for porous ductile media, J. Eng. Mater. Technol. 99 (1977) 2–15.
[4] J. Lee, J. Oung, Yield functions and flow rules for porous pressure-dependent strain-hardening polymeric materials, J. Appl. Mech. 67 (2000) 288–297.
[5] T.F. Guo, J. Faleskog, C.F. Shih, Continuum modeling of a porous solid with pressure sensitive dilatant matrix, J. Mech. Phys. Solids 56 (2008) 2188–2212.
[6] P. Thoré, F. Pastor, J. Pastor, Hollow sphere models, conic programming and third stress invariant, Eur. J. Mech. A, Solids 30 (2011) 63–71.
[7] M. Gologanu, J. Leblond, Approximate models for ductile metals containing non-spherical voids – case of axisymmetric prolate ellipsoidal cavities, J. Mech. Phys. Solids 41 (11) (1993) 1723–1754.
[8] M. Gologanu, J. Leblond, G. Perrin, J. Devaux, Approximate models for ductile metals containing non-spherical voids – case of axisymmetric oblate ellipsoidal cavities, J. Eng. Mater. Technol. 116 (1994) 290–297.
[9] M. Garajeu, P. Suquet, Effective properties of porous ideally plastic or viscoplastic materials containing rigid particles, J. Mech. Phys. Solids 45 (1997) 873–902.
[10] V. Monchiet, E. Charkaluk, D. Kondo, An improvement of Gurson-type models of porous materials by using Eshelby-like trial velocity fields, C. R. Mecanique 335 (2007) 32–41.
[11] V. Monchiet, O. Cazacu, E. Charkaluk, D. Kondo, Macroscopic yield criteria for plastic anisotropic materials containing spheroidal voids, Int. J. Plast. 24 (2008) 1158–1189.
[12] V. Monchiet, E. Charkaluk, D. Kondo, Macroscopic yield criteria for ductile materials containing spheroidal voids: an Eshelby-like velocity fields approach, Mech. Mater., http://dx.doi.org/10.1016/j.mechmat.2013.05.006.
[13] H. Thai-The, P. Francescato, J. Pastor, Limit analysis of unidirectional porous media, Mech. Res. Commun. 25 (1998) 535–542.
[14] P. Francescato, J. Pastor, B. Riveill-Reydet, Ductile failure of cylindrically porous materials. Part I: Plane stress problem and experimental results, Eur. J. Mech. A, Solids 23 (2004) 181–190.
[15] J. Pastor, P. Francescato, M. Trillat, E. Loute, G. Rousselier, Ductile failure of cylindrically porous materials. Part II: Other cases of symmetry, Eur. J. Mech. A, Solids 23 (2004) 191–201.
[16] M. Trillat, J. Pastor, Limit analysis and Gurson's model, Eur. J. Mech. A, Solids 24 (2005) 800–819.
[17] J. Salençon, Calcul à la rupture et analyse limite, Presses des Ponts et Chaussées, Paris, 1983.
[18] E. Anderheggen, H. Knopfel, Finite element limit analysis using linear programming, Int. J. Solids Struct. 8 (1972) 1413–1431.
[19] K. Krabbenhoft, A. Lyamin, M. Hijaj, S. Sloan, A new discontinuous upper bound limit analysis formulation, Int. J. Numer. Methods Eng. 63 (2005) 1069–1088.
[20] F. Pastor, Résolution par des méthodes de point intérieur de problèmes de programmation convexe posés par l'analyse limite, thèse de doctorat, facultés universitaires Notre-Dame-de-la-Paix, Namur, Belgium, 2007.
[21] F. Pastor, E. Loute, J. Pastor, M. Trillat, Mixed method and convex optimization for limit analysis of homogeneous Gurson materials: a kinematical approach, Eur. J. Mech. A, Solids 28 (2009) 25–35.
[22] A. Makrodimopoulos, C.M. Martin, Upper bound limit analysis using discontinuous quadratic displacement fields, Commun. Numer. Methods Eng. 24 (2008) 911–927.
[23] MOSEK ApS, C/O Symbion Science Park, Fruebjergvej 3, Box 16, 2010 Copenhagen ϕ, Denmark, http://www.mosek.com, 2010.
[24] P. Thoré, F. Pastor, J. Pastor, D. Kondo, Closed form solutions for the hollow sphere model with Coulomb and Drucker–Prager materials under isotropic loadings, C. R. Mecanique 337 (2009) 260–267.